Experimental Investigation and Modeling of the Impact of Random Packings on Mass Transfer in Fluidized Beds

Powder Technology 440 (2024) 119781

Contents lists available at ScienceDirect

Powder Technology

journal homepage: www.journals.elsevier.com/powder-technology

Experimental investigation and modeling of the impact of random packings on mass transfer in fluidized beds

Nasrin Nemati *, David Pallarès, Tobias Mattisson, Diana Carolina Guío-Pérez, Magnus Rydén

Division of Energy Technology, Department of Space, Earth and Environment, Chalmers University of Technology, Göteborg, Sweden

HIGHLIGHTS

- Some challenges of fluidization of Geldart B particles: bubbles coalescence and growth.
- Phenomena from bubbles coalescence: reduced mass transfer in fluidized beds.
- The use of random packings in a fluidized bed could break down bubbles successfully.
- Studies of packed-fluidized beds with evolved packing are vital in bubbling fluidization.
- Random metal packings increase mass transfer successfully in bubbling fluidized bed.

GRAPHICAL ABSTRACT

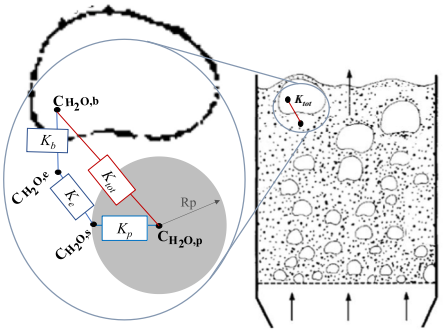

ARTICLE INFO

Keywords:
Fluidization
Gas-solids mass transfer
Packed-fluidized bed
Confined fluidization

ABSTRACT

This study investigates the impact of two novel settings of bubbling fluidized beds equipped with random metal packings on the mass transfer. To do this, a comprehensive approach is applied that integrates experiments and modeling and explores the relevance of the different underlying mechanisms involved in interphase mass transfer in fluidized beds. Firstly, the mass transfer of water from moisturized silica gel particles to dry air is studied in both a packed-fluidized bed and a freely bubbling bed with no packing. The experimental set-up consists of a cylindrical bubbling fluidized-bed column with an inner diameter of 22 cm. Silica-gel particles with a mean particle diameter of 797 μm are used as bed material. The total bed amount ranges from 4 to 8 kg, while the fluidization number (F) varies between 1.7 and 2.3. Two types of packing, RMSR (stainless steel thread saddle rings) and Hiflow (stainless steel pall rings) are examined and compared to the reference case of a bubbling bed with no packing. The height of the packed section is maintained at 60 cm. The results show that, at all operating conditions, the use of packings enhances the amount of desorbed water in the fluidized bed. The increase is up to 17%, as compared to the bed without packing. The effect is believed to be inhibition of bubble growth in the packed-fluidized bed. To study this further, a mass-transfer model is introduced to analyze the different mass-transfer steps (intra-particle, particle surface to emulsion gas, and emulsion gas to bubble gas) in packed-fluidized beds compared to beds with no packing. TGA experiments are applied to describe the intra-particle mass transfer through a desorption kinetic model. Model analysis shows that the main resistance for mass transfer occurs across the bubble-emulsion boundary. The calculated value of the mass transfer coefficient for

* Corresponding author.
E-mail address: nasrinn@chalmers.se (N. Nemati).

https://doi.org/10.1016/j.powtec.2024.119781
Received 16 January 2024; Received in revised form 16 April 2024; Accepted 16 April 2024
Available online 18 April 2024

this, K_b, at reference conditions (6 kg of silica gel and F = 2.3) is 7.6e-5 s^{-1} with packings (in average) and 6.2e-5 s^{-1} without packings, i.e. a 23% improvement in the governing mass-transfer coefficient.

1. Introduction

Many current and future chemical- and energy-conversion processes utilize interactions between solid particles and gases in fluidized-bed (FB) reactors. Some examples include Fluid Catalytic Cracking, combustion and gasification of solid fuels, Chemical-Looping Combustion (CLC), Chemical-Looping Gasification, and Carbonate Looping. FB technologies are also applied for adsorption, drying, polymerization, etc. For these technologies, in many instances, mass transfer in the fluidized bed can be a rate-limiting step, as has been demonstrated by e.g. Aronsson et al. [1] or Nemati et al [2,3]

For particles classified under Geldart group B [4], beyond the minimum fluidization velocity, u_{mf} (m.s^{-1}), the bed undergoes a transition wherein gas bubbles are formed within the bed. Such a bed is referred to as a bubbling fluidized bed (BFB) [4–6]. In a BFB, an increased gas flow results in an increase in average bubble size and, consequently, an augmented gas throughput within and across bubbles [6], and thus less efficient gas-solids contact [7]. Furthermore, in bubbling beds with a high height-to-diameter ratio, gas bubbles will eventually become large enough to spread across the entire column cross-section, a phenomenon referred to as slugging [6]. Slugging and bubble growth are usually undesirable from the perspective of the gas-solids contact, since the reduced specific surface area of large bubbles or slugs results in a decrease in the mass transfer of gas between bubbles and the emulsion phase [1,8,9]. In the context of CLC, for instance, bubble growth may result in a variety of issues such as incomplete gas conversion, char loss to the air reactor, and the presence of elutriated char in the flue gas [10]. In practice, bubble growth in the CLC fuel reactor is expected to lead to reduced fuel conversion and reduced CO_2 sequestration [11–13].

Several strategies have been suggested and investigated to limit bubble growth and enhance mass transfer in BFB reactors to overcome the aforementioned challenges. Information on the impact of fixed internals (baffles, tubes, or screens) on bubble behavior is significant, see for example Asegehegn et al. [14], Nguyen et al. [15], Mojtahedi [16], and Andersson et al. [17], who demonstrated that fixed internals effectively mitigate the formation of large bubbles and slugs within a bubbling bed, breaking them down into smaller entities. Nonetheless, the incorporation of fixed internals such as e.g. tube bundles in a fluidized bed involves several challenges including erosion, complex maintenance, and potential problems with mechanical stress at elevated temperatures.

One method to eliminate bubble growth in BFBs is by applying the concept of packed-fluidized beds, sometimes also referred to as confined fluidization. In this concept, illustrated in Fig. 1, inert stagnant packings, consisting of immersed objects of much larger size than the fluidized particles, are used to inhibit bubble formation and growth by breaking down larger bubbles into smaller ones.

The concept of packed-fluidized bed was first suggested in 1950 by Matheson [18]. Subsequently, in 1961, Williamson developed the principle by introducing non-fluidized large spheres to impede the downflow of fluidized particles in a multi-stage fluidized bed reactor [19]. Following this, several authors, including Sutherland et al. [20,21], Ziegler and Brazelton [22], and Gabor et al. [23–28], investigated the exploration of employing a few other sorts of packings in fluidized beds such as raschig rings. In 1963, Sutherland et al. investigated the influence of packing materials (spherical, Raschig Ring, and Berl saddle) on the characteristics of a gas-fluidized bed [20]. This study encompassed parameters such as minimum fluidization velocity, u_{mf} (m.s^{-1}), pressure drop, bed expansion, and heat transfer. Two years later, in 1965, Gabor and Mecham [25] studied the use of packed-fluidized beds with spherical packings for the enhanced removal of heat generated during the fluorination of depleted uranium oxide pellets. By incorporating small inert spherical particles in the voids between the uranium pellets, effectively forming a packed fluidized bed, they could enhance the rate of heat transfer. Their findings included observations of increased heat-transfer coefficients in regions sufficiently distant from the walls and upper boundaries of the packing, as well as higher bubble frequencies and consequently increased particle movement in the central region of the packed-fluidized bed.

More recently, other studies about the use of packed-fluidized beds have been presented in the literature, such as examination of bed expansion, pressure drop [29,30], and minimum fluidization conditions [31], but also studying the hydrodynamics of confined fluidization with packing solids [32], and kinetics and mass transfer (for catalytic hydrogenation of ethylene) [33]. These studies have collectively demonstrated the potential advantages of utilizing packed-fluidized beds in various contexts, mainly applying spherical packings.

Recently, Nemati et al. [2,3,34] have undertaken investigations into the effects of different packings during CLC batch experiments. These studies reported that a new sort of metal packings like RMSR (stainless steel thread saddle rings) and Hiflow (stainless steel pall rings) can enhance the fuel conversion rate in CLC, as compared to conventional fluidized beds with no packing. However, the underlying theoretical basis supporting these observations remains unclear. Furthermore, additional investigations on the impact of these packings on the hydrodynamics of the fluidized bed are deemed necessary in order to clarify their influence on mass transfer in the fluidized bed.

1.1. Aim of this study

The main purpose of this study is to determine the impact of random metal packings on the gas-solids mass transfer in a bubbling fluidized bed. To achieve this aim, targeted experiments in a bed of moist silica gel are performed, in which the rate of H_2O desorption is monitored for free bubbling and fluidized-packed bed conditions. Detailed analysis of the mass transfer is done through a model accounting for the different steps in the mass transfer chain. All previous work in packed-fluidized beds is largely focused on pure experimental investigations, with limited

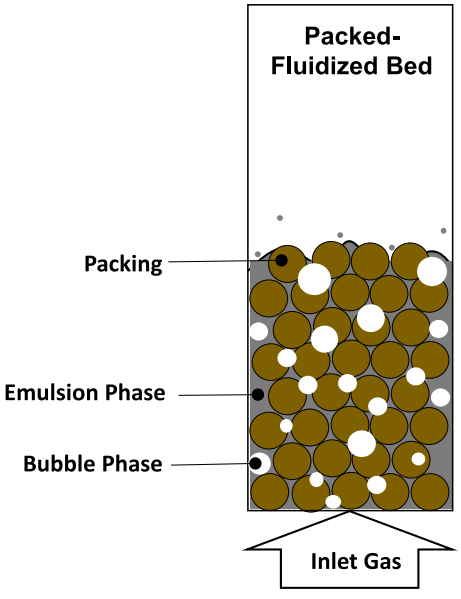

Fig. 1. Illustration of packed-fluidized bed (or confined fluidized bed).

modeling to support experiments. Hence, in terms of novelty this work contributes by both i) for the first time coupling experiments with detailed modeling of the important mass-transfer of gas in the fluidized bed, ii) applying a new setting of bubbling fluidized beds equipped with random packings (non-spherical) not previously studied.

2. Materials and methods

2.1. Bed material and packings

Silica gel particles are selected as bed material due to their high moisture adsorption capacity. The bulk density of the silica gel particles was measured to 680 kg.m^{-3}, and the particles were sieved to the size range of 355–2100 μm (Fig. 2), resulting in a Sauter particle diameter of 797 μm.

The minimum fluidization velocity of the silica gel particles (in the bed with no packing) is determined experimentally (details are provided in the supplementary material, Fig. S1), leading to a value of 0.15 m.s^{-1}. It is assumed that this property is not altered by the presence of packings. This assumption is done based on a previous work by the authors [34] with packed-fluidized beds showed that the presence of RMSR and Hiflow packings in the bed had a marginal effect on the pressure drop and u_{mf}, due to the high void factor of the packings.

Packings employed in the study are 25-mm stainless-steel thread saddles (RMSR) and 25-mm stainless-steel pall rings (Hiflow) (Fig. 3). For RMSR, the nominal bulk density and void factor are 232 kg.m^{-3} and 0.97, respectively. For Hiflow, the corresponding values are 390 kg.m^{-3} and 0.95. More information about the packings is provided in previous studies [2,3,34].

2.2. FB experimental set-up

The experiments are carried out in a transparent cylindrical acrylic column of 1.5 m in height and an inner diameter of 22 cm. The column is equipped with two humidity sensors (Vaisala Combined Pressure, Humidity, and Temperature Transmitter, PTU300) to sample water content in the input and outlet gas (Fig. 4).

The gas distributor consists of a perforated steel plate with a metal mesh layer impeding the leakage of particles into the windbox. The air distributor plate has 190 holes with a diameter of 1 mm in a triangular pitch arrangement. Elutriated particles are collected in a filter installed downstream. The reactor has 13 pressure-measurement taps located at different heights connected to Huba Control transducers, which feed into a NiDAQ A/D converter and are logged using NI LabVIEW.

Upstream from the column inlet, the system consists of a mass flow controller, a heater, and a humidifier. Through the mass flow controller, the superficial gas velocity directed to the FB is controlled. A practical

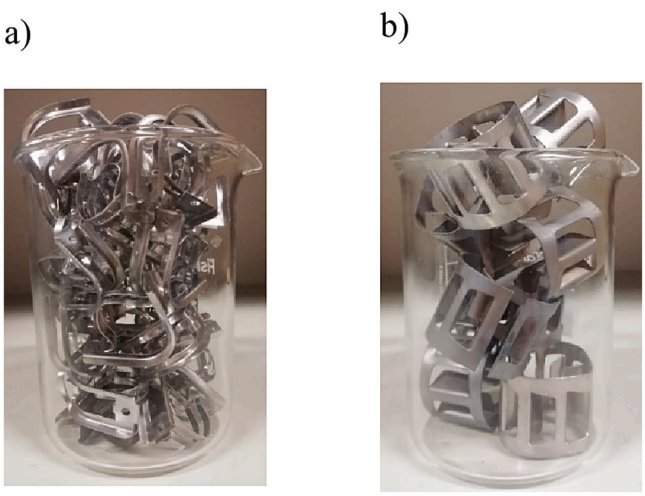

Fig. 3. Packings investigated in this study: a) RMSR, b) Hiflow.

method to characterize this superficial gas velocity in the BFB is by employing the dimensionless Fluidization number (F). This parameter represents the ratio between the superficial gas velocity and u_{mf} (m.s^{-1}). The humidifier is constructed from industry-grade PVC piping. The pipe has a 16 cm outer diameter and a height of 2 m. Closure caps are fixed at both ends of the pipe. At the upper cap, two openings are mounted to serve as inlet points for dry air, while one opening is designated as the exit for the humidified air at the top. Inside the pipe, the dry air inlets are connected to tubing of approximately equivalent length as the pipe, so that air is added at the bottom of the column. These tubes are perforated at their bottom sections. The design enables dry air to rise as bubbles through a column of water and undergo humidification.

2.3. Experimental procedure

2.3.1. FB experiments

For the experiments with packings, the FB reactor is first loaded with packings up to a height of 60 cm. Following that, the system is filled with 4 kg of silica gel. Then, the superficial gas velocity is set to 0.25 m.s^{-1}, which corresponds to a fluidization number of F = 1.7. Subsequently, the inlet air temperature is regulated to 30 °C employing a pre-heater, before its introduction into the humidifier. Owing to heat losses to the environment in the humidifier and the piping before the bed, the fluidized bed exhibits a slightly lower temperature. At steady state, the inlet air temperature is around 25 °C. Due to the high heat capacity of the FB [35,36], both adsorption and desorption in this study can be

355	0
500	4.21
710	33.89
1180	97.56
1800	100
2100	100

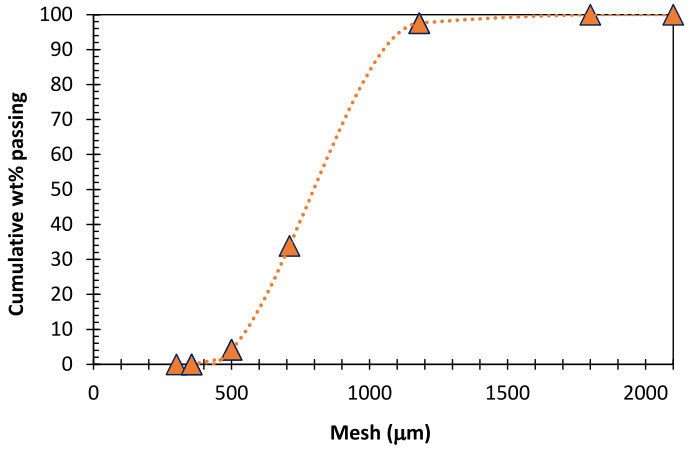

Fig. 2. Silica gel particles size distribution.

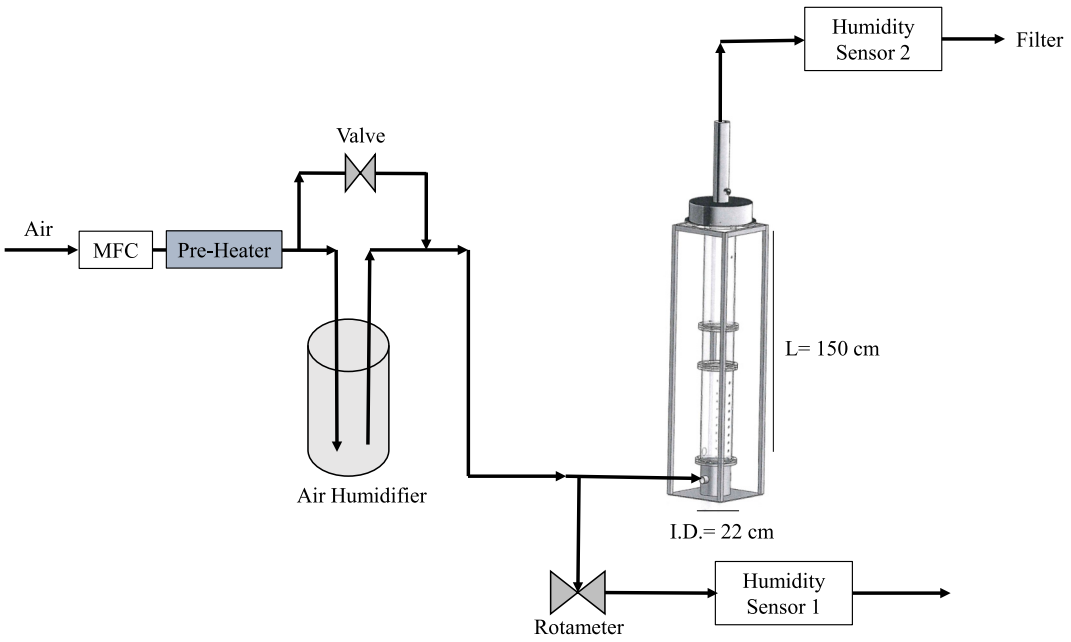

Fig. 4. Schematic diagram of experimental setup.

treated as isothermal processes (see Fig. S2 in the supplemental section for examples of the temperature in the FB throughout the desorption process as empirical confirmation).

After approximately four hours, the humidity becomes steady at both the inlet and outlet of the FB column, meaning that the silica gel can be considered saturated. The inlet air is then switched from humidified to dry, thus starting the desorption process. The absolute humidity in the inlet and outlet of the FB column are then logged for approximately three hours. The step-by-step experimental procedure is summarized in Table 1.

A series of experiments are performed, varying the amounts of bed material and the fluidization number, see Table 2 for a detailed test matrix.

As depicted in Table 2, different settled bed heights and fluidization numbers, *F*, have been examined for RMSR packings and compared with an unpacked bed configuration. Due to the comparable properties between the investigated packings in terms of their void factor and the observed relatively low impact on the results, one data point in the average range was selected and studied for the Hiflow packing for the experiments.

2.3.2. TGA experiments

The adsorption capacity and desorption kinetics of silica gel particles are determined by experiments in a thermogravimetric analyzer (TGA) with a sensitivity of 0.1 μg. A detailed description of the TGA apparatus can be found elsewhere [37]. For these experiments, a sample of 2.5 mg of dry silica gel is loaded onto the platinum plate. The atmosphere is of 90 mL.min^{-1} air/or N_2 and 10 mL.min^{-1} purge flow. Table 3 presents the procedure followed for TGA experiments in this study.

Table 1
The experimental procedure.

Step	Procedure
1. Saturation	- Add the desired quantity of silica gel particles and packings to the reactor. - Humidify the FB with humidified air at 30 °C, until the measured humidity is steady both at the reactor inlet and reactor outlet.
2. Desorption	- Switch from humidified air to dry air to begin the desorption experiments and collect data for approximately three hours.
3. Data evaluation	- Stop the desorption experiments after the data collection step and analyze the results.

2.4. Data evaluation

The instantaneous water desorption rate can be determined from measurements as Eq. (1), with the assumption that the flows in and out are similar.

$$\dot{m}(t) = G_{air}\left(H_{out}^{abs}(t) - H_{in}^{abs}(t)\right) \quad (1)$$

The total quantity of water desorbed from silica gel particles throughout the drying experiments is determined from the time-integration of humidity data as:

$$\Delta m_{des} = \int_0^{t_f} \dot{m}(t)dt \quad (2)$$

In this work, a desorption analysis time of $t_f = 2$ h was found suitable for the data analysis, as longer time frames provided no additional information.

The adsorption capacity, B_{ads}, of silica gel particles is defined as the mass ratio between the maximum amount of adsorbed water (step 5 in Table 3) and the dry silica gel particles (step 4 in Table 3) (Eq. (3)):

$$B_{ads} = \frac{m_{p,sat} - m_{p,dry}}{m_{p,dry}} \quad (3)$$

3. Modeling the desorption process

In this section, the model for desorption in gas-fluidized beds is presented. A standard volumetric mass transfer coefficient, K_{tot}, is used to describe the overall mass transfer rate of water between the particles and the gas in the bubble phase, as suggested by e.g. Kunii and Levenspiel [6]:

$$\dot{m}(t) = K_{tot} V_R \left(C_{H2O,p} - C_{H2O,b}^{avg}\right) \quad (4)$$

where, V_R is the reactor volume, $C_{H2O,p}$ is the concentration of water in the particle, and $C_{H2O,b}^{avg}$ is the average water concentration in the bubble phase.

The overall mass transfer coefficient, K_{tot}, can be broken down into the three constitutive sequential steps, as illustrated in Fig. 5: i) the

Table 2
Test matrix used in this work.

No.	Packing			Bed inventory		Air flow	
	type	Packing void factor (−)	Packing height (cm)	mass (kg)	Settled bed height (cm)	Superficial gas velocity (m.s^{-1})	Fluidization number (F) (−)
1		1	_	4	15.5	0.25	1.7
2		1	_	4	15.5	0.35	2.3
3	No packing	1	_	6	23.2	0.25	1.7
4		1	_	6	23.2	0.35	2.3
5		1	_	8	31.0	0.25	1.7
6		0.96	60	4	16.3	0.25	1.7
7		0.96	60	4	16.3	0.35	2.3
8	RMSR	0.96	60	6	24.4	0.25	1.7
9		0.96	60	6	24.4	0.35	2.3
10		0.96	60	8	32.6	0.25	1.7
11	Hiflow	0.95	60	6	24.2	0.35	2.3

Table 3
The procedure followed for TGA experiments.

Step	Procedure	Duration (min)	Purpose
1	Ramp 5 °C/min to 100 °C	15	Increasing the temperature to 100 °C
2	Isothermal with dry air at 100 °C	30	Exposure of particles to dry air at 100 °C
3	Change the temperature to 25 °C	–	Changing Temperature to 25 °C with dry air
4	Isothermal with dry air at 25 °C	195	To reach a steady-state condition at 25 °C
5	Isothermal with saturated air at 25 °C	180	Moisturizing silica gel with saturated air at 25 °C
6	Isothermal with dry air at 25 °C	285	Desorption of water from silica gel with dry air at 25 °C
7	Ramp 5 °C/min to 100 °C	15	Increasing the temperature to 100 °C
8	Isothermal with dry air at 100 °C	30	Drying the particles with dry air at 100 °C
9	Isothermal with Nitrogen at 100 °C	30	Drying the particles with Inert N_2 at 100 °C
10	Ramp 5 °C/min to 25 °C	15	Cooling down the system

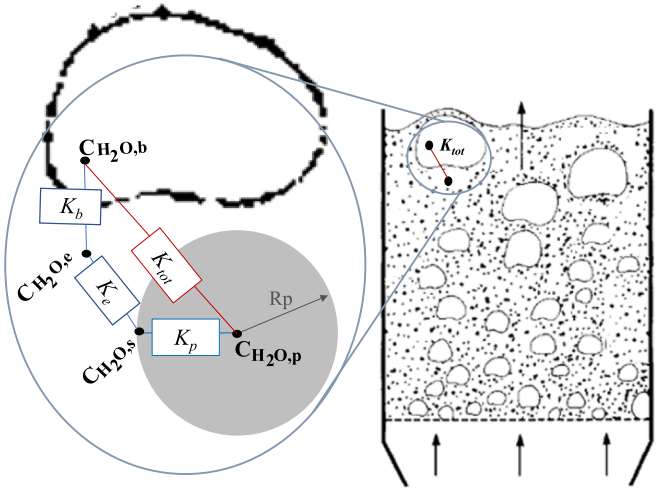

Fig. 5. The nature of and relationship of the mass-transfer coefficients examined in this work.

transfer of water from internal particle sites to the particle surface (which entails both kinetics and intra-particle mass transfer and is characterized through the transfer coefficient K_p), ii) the mass transfer of gas across the boundary between the particle surface and the emulsion gas (characterized through the coefficient K_e), and iii) the mass transfer from the emulsion gas to the bubble phase (characterized through the coefficient K_b). The relationship between the coefficients for each of these three contributing mechanisms and the resulting coefficient for the overall mass transfer, K_{tot}, is given by the series-coupling expression given in Eq. (5), formulated following principles delineated in Kunii and Levenspiel [6].

$$\frac{1}{K_{tot}} = \frac{1}{K_p} + \frac{1}{K_e} + \frac{1}{K_b} \tag{5}$$

In this work, the presence of packings in the fluidized bed is assumed to not affect the intra-particle mass transfer, K_p (which is linked to the intra-particle properties of the silica gel), nor the mass transfer between the particle surface and the emulsion gas, K_e (which is influenced only by the microscopic flow conditions in the immediate surrounding of each bulk particle). Thus, the presence of packings is assumed to impact solely the emulsion-bubble mass transfer by means of affecting the characteristics of the bubble flow (smaller bubbles, and thus a higher specific surface area of the bubble phase). However, the presence of packing in FB affects the characteristics of the bubble flow. This leads to a change in the specific surface area of bubbles. Thereby K_b and thus also eventually the overall mass transfer, K_{tot} will change. In this work, K_p is established through TGA experiments (see Section 3.1), while K_e is estimated using well-established correlations in literature [38] (see Section 3.2). With these two determined, evaluation of K_{tot} allows determination of K_b (through Eq. (5)) and thus analysis of the impact of packings on this mass transfer step.

Closure of the mass balance involves consideration of the two-phase theory [6] of fluidization, illustrated in Fig. 6, and stating that the gas flow through the emulsion equals that required for minimum fluidization, while all gas in excess of that will flow in the form of bubbles. From this, the sampled outlet gas concentration can be broken down into the contributions of each gas phase (emulsion and bubbles), see Eq. (6). Note that while at fluidization velocities well above the minimum fluidization velocity, i.e. so-called well-agitated beds, the emulsion phase contribution can be neglected, this is not reasonable for low fluidization numbers.

$$C^{out}_{H2O} = C^{out}_{H2O,e}\,\frac{u_{mf}}{u} + C^{out}_{H2O,b}\,\frac{u-u_{mf}}{u} \tag{6}$$

Assuming well-mixed solids, the average gas concentration along the bed height in the emulsion, $C^{avg}_{H2O,e}$, phase is expressed as the logarithmic mean of the corresponding inlet and outlet concentrations, i.e.:

$$C^{avg}_{H2O,e} = \frac{\left(C^{out}_{H2O,e} - C^{in}_{H2O,e}\right)}{ln\frac{C^{out}_{H2O,e}}{C^{in}_{H2O,e}}} \tag{7}$$

Further, to determine the system of equations formed by Eqs. (1) and (4)–(7). the expression assessing the water transfer between the particle and the emulsion must be considered. This is done by accounting for the intra-particle rate of diffusion, K_p, and the particle-emulsion transfer rate, K_e, in the driving concentration difference between the particle and

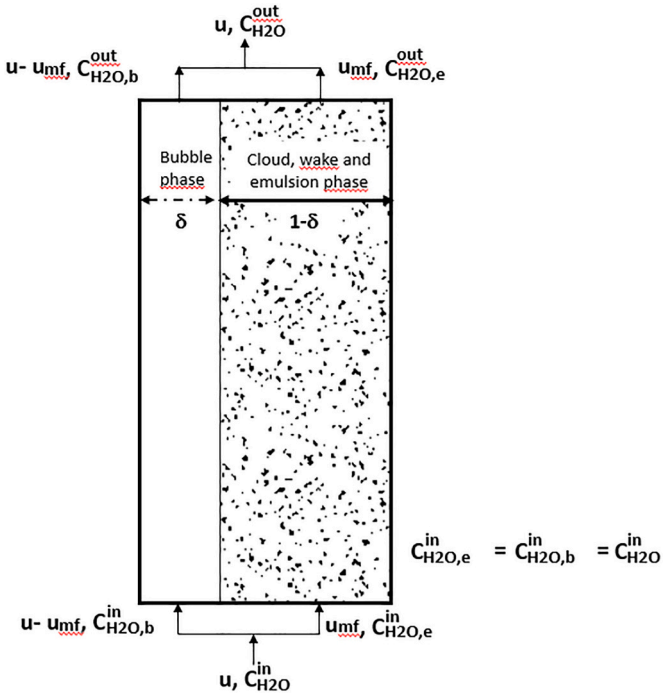

Fig. 6. The two-phase theory model of fluidization.

the emulsion phase:

$$\dot{m}(t) = \frac{1}{\frac{1}{K_P} + \frac{1}{K_e}}\, \varepsilon V_R \left(C_{H2O,p} - C^{avg}_{H2O,e}\right) \tag{8}$$

At any time, the concentration of water in the particles, $C_{H2O,p}$ is calculated according to the current amount of water contained in the particles [35,36], i.e.:

$$C_{H2O,p} = \frac{m_p(t) - m_{p,dry}}{m_{p,sat} - m_{p,dry}} \times C_{p,sat}(t=0) \tag{9}$$

As mentioned above, K_p and K_e are determined by TGA experiments and literature expressions, respectively (see Sections 3.1 and 3.2). With this, for each time step, Eq. (8) facilitates the calculation of $C^{avg}_{H2O,e}$. Following this, the determination of $C^{out}_{H2O,e}$, and $C^{out}_{H2O,b}$ is ascertained through Eq. (7) and Eq. (6), respectively. Lastly, by knowing $C^{out}_{H2O,b}$, $C^{ave}_{H2O,b}$ is obtained by employing logarithmic average for bubble phase similar to Eq. (7).

3.1. Intra-particle mechanisms (K_p)

To determine K_p, experimental data from experiments in TGA is used (step 6 in Table 3). In this step, the saturated silica gel particles are exposed to dry air at 25 °C and the degree of water desorption at each given time, X (−), is calculated as:

$$X = 1 - \frac{m_p(t) - m_{p,dry}}{m_{p,sat} - m_{p,dry}} = \frac{m_{p,sat} - m_p(t)}{m_{p,sat} - m_{p,dry}} \tag{10}$$

The degree of water desorption is described as the fraction of the total water loss in the desorption process and increases from 0 to 1 with desorption time. In this study, the desorption data has been analyzed within the conversion degrees spanning from 0.12 to 0.6.

The desorption kinetics from particles can be parametrized for three variables: temperature $K^*_p(T)$, the extent of conversion $g(X)$, and the partial pressure of water $p_{H2O}(p)$ [39,40]:

$$\frac{dX}{dt} = K^*_p\, g(X) \left(1 - \frac{p_{H2O}}{p_{H2O,SAT}}\right) \tag{11}$$

For the TGA experiments, the concentration of water vapor in the gas phase (p_{H2O}) is considered negligible, since the atmosphere in the chamber is continuously renewed with dry air. This was confirmed by observing the same mass loss data at increased purging flow rates. Thus, for the TGA experiments, Eq. (11) can be reformulated as follows to derive the internal kinetics within the particles:

$$\frac{dX}{dt} = K^*_p\, g(X) \tag{12}$$

A gathering of g(X)-expressions from the kinetics committee of the International Confederation for Thermal Analysis and Calorimetry (ICTAC) [40] is shown in Table 4.

Table 4 shows also the integral form of the conversion terms, *F(X)*, which is more suitable for analysis of experimental data and which Sharp et al. [41] presented as:

$$F(X) = \int_0^X \frac{dX}{g(X)} = \alpha\left(\frac{t}{t_{0.5}}\right) \tag{13}$$

where, α (−) represents a constant and $t_{0.5}$ is the time corresponding half-termed conversion ($t_{0.5}$ = 215 s). For this work, the evaluation process commences by assessing Eq. (13) applied to the experimental dataset, denoted as (t(s), X(−)), which has been acquired through TGA. Concurrently, various *F(X)* models, as listed in Table 4, are evaluated. The selection of the most compatible *F(X)* model with the experimental data is subsequently made.

Thus, once a *g(X)* model is selected the mass loss rate in the TGA can be expressed as:

$$\dot{m}(t) = -\left(m_{p,dry} - m_{p,sat}\right) K^*_p\, g(X) \tag{14}$$

In the FB scale, the mass loss rate of a concentration-driven mass transfer scheme governed by intra-particle mechanisms can be expressed in terms of a volumetric mass transfer coefficient as shown in Eq. (15). Note that the average water concentration in the particle is expressed as $C_{H2O,p}$=$C_{p,sat}(1-X)$:

$$\dot{m}(t) = K_P\, V_R \left(C_{H2O,p} - C_{H2O,s}\right) = K_P\, V_R \left(C_{p,sat}(1-X) - C_{H2O,s}\right) \tag{15}$$

Equating the two above expressions and accounting that $C_{H2O,s} \approx 0$ in the TGA experiments, the following is obtained:

$$K_P = -K^*_p \frac{g(X)}{1-X} \frac{m_{p,dry} - m_{p,sat}}{V_R\, C_{p,sat}} = K^*_p \frac{g(X)}{1-X} \tag{16}$$

Table 4
Kinetic models used for the desorption of silica gel particles [39–41].

Kinetic model	g(X) (−)	F(X) (−)	α (−)
Diffusion-controlled			
One-dimentional diffusion (D1)	$1/2\times^{-1}$	X^2	0.2500
Two-dimentional diffusion (D2)	$[-\ln(1\text{-}X)]^{-1}$	(1-X)ln(1-X) + X	0.1534
Three-dimentional diffusion (D3)	$3/2(1\text{-}X)^{2/3}[1\text{-}(1\text{-}X)^{1/3}]^{-1}$	$[1\text{-}(1\text{-}X)^{1/3}]^2$	0.0426
Moving phase-boundary controlled			
Contracting cylinder or disk (R2)	$2(1\text{-}X)^{1/2}$	$1\text{-}(1\text{-}X)^{1/2}$	0.2929
Contracting sphere (R3)	$3(1\text{-}X)^{2/3}$	$1\text{-}(1\text{-}X)^{1/3}$	0.2063
Kinetic Equation based on the concept of first order of reaction			
Mampel (first order) (F1)	1-X	-ln(1-X)	0.6931
Avrami-Erofe'ev Equations			
Avrami-Erofeev (A2)	$2(1\text{-}X)[-\ln(1\text{-}X)]^{1/2}$	$[-\ln(1\text{-}X)]^{1/2}$	0.8326
Avrami-Erofeev (A3)	$3(1\text{-}X)[-\ln(1\text{-}X)]^{2/3}$	$[-\ln(1\text{-}X)]^{1/3}$	0.8850

3.2. Mass transfer from particle surface to emulsion gas (K_e)

In this study, a Frössling-type correlation was selected to describe the mass transfer from particle surface to emulsion gas in the FB, due to its strong alignment with experimental data in the literature [42]:

$$Sh = \frac{k_e d_p}{D} = 2\varepsilon_{mf} + 0.7\left(\frac{Re_{mf}}{\varepsilon_{mf}}\right)^{1/2} Sc^{1/3} \quad (17)$$

The Frössling-type correlation's validity was supported by Scala's research involving CO oxidation over a Pt catalyst in a bubbling FB [38]. Within this correlation, it is highlighted that the Sherwood number (*Sh*) remains unaffected by fluidization velocity, while it exhibits a square root relationship with the minimum fluidization velocity, u_{mf} ($m.s^{-1}$), and thus particle size. Scala's observations suggest that active particles are exclusively present in the dense phase and do not transition into the bubble phase. Moreover, the particle density does not exert a significant influence on *Sh* according to his findings.

Finally, it must be noted that, for a sphere, mass transfer coefficients can be converted between surface-based (k_e ($m \bullet s^{-1}$) obtained from Eq. (17)) and volume-based (K_e (s^{-1})) values through the following equivalence:

$$K_e = \frac{k_e A_p}{V_p} = \frac{k_e\, 6}{d_p} \quad (18)$$

4. Results and discussion

4.1. Adsorption capacity of silica gel

Fig. 7 illustrates the outcomes of six consecutive TGA cycles. The numbers on the top of the diagram indicate each step, as outlined in Table 3. While cycle 1 shows a distinctly larger adsorption capacity, the adsorption capacity remains unchanged for the following cycles. This shows that the silica gel particles result in a stable reactivity from the second cycle. Based on Eq. (3), the adsorption capacity of the examined silica gel is calculated to be $B_{ads} = 0.277$ (−).

4.2. Effective mass transfer in FB

The absolute humidity at the outlet of the FB under desorption experiments involving 6 kg silica gel and F = 2.3 is depicted in Fig. 8 for three different cases (no packings and packing of two types). For these experiments, silica gel was first saturated with humidified air holding 12–14 $g_{H2O}/m^3_{dry\ air}$. Then the inlet air was switched from humidified to atmospheric air (here called also dry air) with 0.4 $g_{H2O}/m^3_{dry\ air}$.

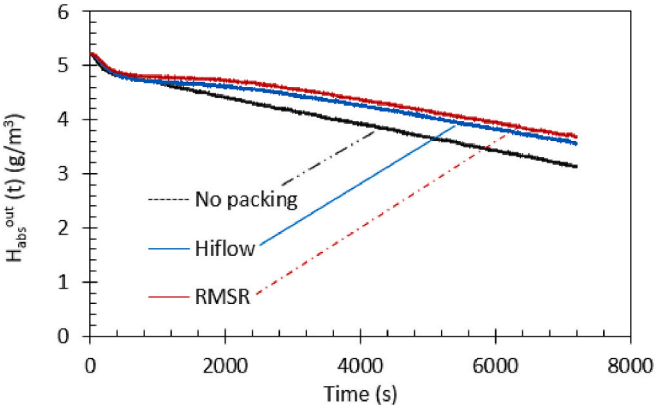

Fig. 8. Absolute humidity of the outlet air as a function of time, 6 kg silica gel, F = 2.3.

Regarding the outlet air (as shown in Fig. 8), during the initial phase of the experiments (0–1000 s), all three cases exhibited comparable levels of saturation at the experiment's outset. However, in the absence of packing material, a steep decline in outlet humidity ensued shortly thereafter. In contrast, both the RMSR and Hiflow configurations maintained higher outlet absolute humidity levels for an extended duration, persisting until approximately 3000 s. This behavior reflects the higher mass-transfer rate occurring between the silica gel particles and the dry air within the packed-fluidized cases compared to the unpacked bed.

Additionally, data in Fig. 8 makes it evident that the water concentration in the outlet gas - roughly 3–5 $g_{H2O}/m^3_{dry\ air}$ - remains considerably lower than the saturation concentration in air under the operating conditions - 17.8 $g_{H2O}/m^3_{dry\ air}$. This implies that the air does not become saturated and thus the presence of the driving force for desorption, i.e. the mass transfer from the particles to the gas, is confirmed throughout the experiment time.

Table 5 depicts the resulting amount of desorbed water for the different cases examined. As seen, the amount of desorbed water is always larger when packings are applied compared to the unpacked case. This confirms that the presence of packing in the bed improves the mass-

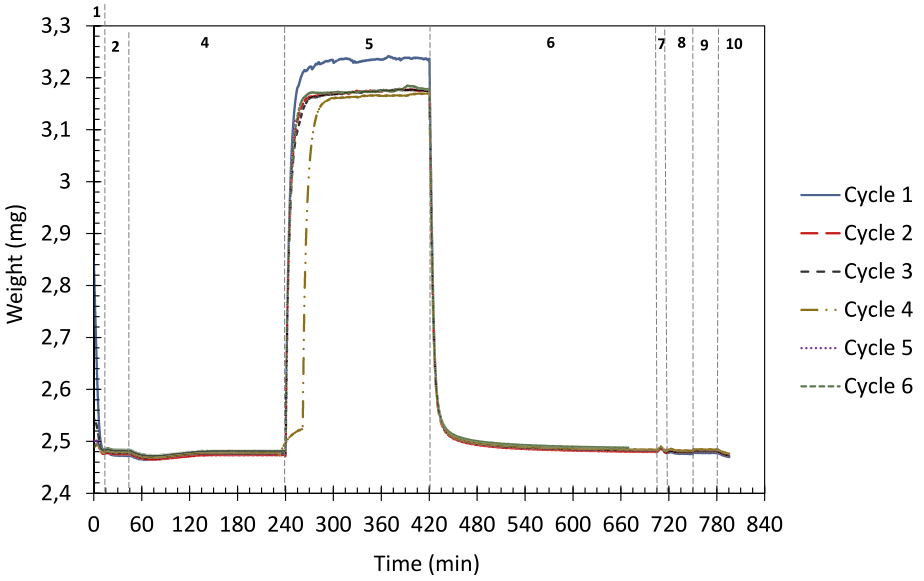

Fig. 7. TGA experiments for 6 cycles.

Table 5
The total value of desorbed water from silica gel particles (Eq. (2)).

No.	Packing	Fluidization number (F) (−)	Superficial gas velocity (m. s^{-1})	Silica gel (kg)	Amount of desorbed water in 6800 s, Δm_{des} (g)	Improvement compared to No packing (%)
1	No packing	1.7	0.25	4	233.0	–
2				6	242.0	–
3				8	261.0	–
4		2.3	0.35	4	280.2	–
5				6	308.4	–
6	RMSR	1.7	0.25	4	261.0	12.0
7				6	276.0	14.0
8				8	281.0	7.7
9		2.3	0.35	4	330.1	17.8
10				6	361.0	16.9
11	Hiflow	2.3	0.35	6	360.3	16.8

transfer compared to a bed with no packing.

For F = 1.7, Comparing 4 kg of silica gel with RMSR and beds without packing in Table 5, demonstrates an approximate 12% enhancement in the quantity of desorbed water into the bubble phase for packed-fluidized beds. Increasing the amount of silica gel from 4 kg to 6 kg results in an augmented overall desorbed water quantity for both RMSR-equipped beds and unpacked beds. Nonetheless, this increase for the bed with RMSR exceeds that of unpacked beds by 14%. Similarly, this improvement is still notable at 7.7% when increasing the amount of silica gel to 8 kg.

For F = 2.3, when RMSR packing is utilized in the fluidized bed, the amount of desorbed water increases by around 17% for each quantity of silica gel compared to a bed with no packing. When comparing F = 1.7 and F = 2.3, it is clear that the benefits in mass-transfer of using packings are more pronounced in beds with higher gas velocities. This can be attributed to the packing's ability to inhibit bubble growth in the bed for such conditions.

Comparing between the two types of packings, both improve the amount of desorbed water by 17% compared to the non-packed base scenario.

4.3. Mass-transfer interchange coefficients

As explained in Section 3, the existence of packings within the FB does not influence the mass transfer inside the particle (K_p), or mass transfer between the particle surface and the surrounding emulsion gas (K_e). Thus, these two coefficients can be determined and used for analysis of the mass transfer between emulsion gas and bubble phase gas (K_b).

The intraparticle coefficient, K_p, is determined by TGA experiments (see Section 3.1). To achieve this, the different conversion models categorized in Table 4 are investigated and compared to the experimental data in Fig. 9, which presents the conversion degree as a function of relative time. As seen, the Mample model (*F1*) demonstrated excellent fit and is thus confirmed as an appropriate choice for representing the desorption kinetics.

Having the Mample model (*F1*) as the best fit to measurement data means g(X) = 1-X (see Table 4). Substituting this into Eq. (16) yields $K_p = K_p{}^*$. The value of $K_p{}^*$ calculated along the progress of desorption is plotted in Fig. 10. As seen, during the initial stages of desorption, K_p stands at zero due to the absence of desorption activity. However, after reaching $X = 0.12$, K_p stabilizes at an approximate value of 4e-3 s^{-1}. This steady value of K_p remains relatively constant until a very late conversion stage ($X = 0.9$), reinforcing the validity of the kinetic model. Beyond this point, K_p experiences a subsequent increase due to the diminishing driving force for desorption ($C_{H2O,p}$-$C_{H2O,s}$). Hence, for the purpose of this study, the chosen value is K_p = 4e-3 s^{-1}, considering that the conversion degree in the FB experiments remains within the range 0.12–0.6.

For TGA experiments, different flow rates were investigated (further information can be found in Fig. S3 in the supplementary section), since prior studies have shown that decreasing the quantity of particles or increasing the gas flow rate can affect the reaction rate until a point is reached where further changes have no significant impact, as external mass transfer becomes fast enough to be negligible [39,43]. For the evaluated conditions, the gas flow in the TGA did not show any influence

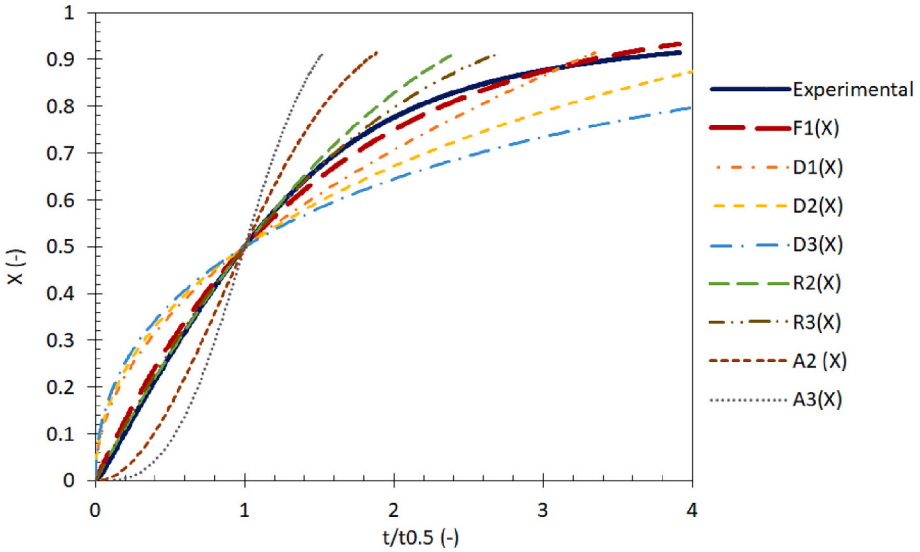

Fig. 9. Conversion as a function of t/t0.5 calculated for various kinetic models in Table 3 (Eq. (13)).

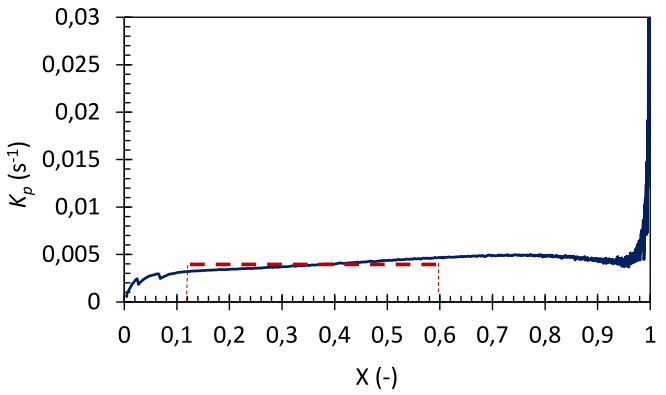

Fig. 10. K_p (S^{-1}) as a function of conversion X (–) for silica gel particles (Eq. (15)). The red line represents X = 0.12–0.6. (For interpretation of the references to colour in this figure legend, the reader is referred to the web version of this article.)

on the mass loss curves, showing that the conversion was governed by intra-particle mechanisms. This aligns with the theoretical exercise of assuming *Sh* to be 1.5 (an average between 2 - when the entire particle is suspended in a stagnant gas - and 1 - when half of the particle is occupied by the tray and is not in touch with the gas. This *Sh*-number for the external mass transfer in the TGA yields $K_{ext} = 339\ s^{-1}$, to be compared with the intra-particle mechanisms, $K_P = 0.004\ s^{-1}$. It is thus obvious also from theory that the intra-particle mechanisms are governing the conversion in the TGA compared to the much faster external mass transfer, which can be neglected.

Regarding the mass transfer between the particle surface and the emulsion gas, the calculation of its coefficient K_e, is carried out utilizing Scala's correlation [38],(Eq. (17)), leading to $Sh = 3.5$, $k_e = 0.1\ m.s^{-1}$, and $K_e = 803.8\ s^{-1}$.

The values of overall mass transfer coefficient, K_{tot}, and the emulsion-to-bubble coefficient, K_b, are calculated based on Eqs. (4) and (5) and presented in Table 6. for the cases investigated. It is important to point out that the emulsion-bubble mass-transfer, is the only parameter that is altered by applying packings.

As seen, from the orders of magnitudes of the coefficients for the different steps, the overall mass transfer is strongly governed by the emulsion-bubble mass-transfer. Further, the emulsion-bubble mass-transfer is seen to be increased by the addition of packings, probably due to the reduced bubble size and consequently increased interface area between bubbles and emulsion. Note that the two different packing types provide the same increase (+23%) in the mass transfer for their common case compared to the unpacked bed condition.

5. Conclusion

This study investigates the possibility to improve mass-transfer in FBs by applying packings - a concept referred to as packed-fluidized bed or confined fluidization. The examined variables are bed inventory (4, 6, and 8 kg), fluidization number (1.7 and 2.3), and packing type (RMSR, Hiflow, or no packings). The key finding is that the use of packings results in a significant increase in mass-transfer rate for all conditions evaluated. Other conclusions are as follows:

- The TGA study of the intra-particle mechanisms for desorption (kinetics and internal mass transfer) shows that the intra-particle mechanisms are governing the desorption in the TGA and can be overlay described based on the Mampel (first order) (*F1*) model, resulting in $K_p = 0.004\ s^{-1}$.
- The desorption experiments in a fluidized bed column are mainly controlled by the mass-transfer between the emulsion gas and the bubble phase, which leads to K_b-values within the range 5.4e-5–10.e-5 s^{-1} and represents almost all of the overall effective mass transfer resistance.
- The inhibition of bubble formation and growth in the packed-fluidized bed increases the emulsion-bubble mass transfer by up to 23% as compared to the bed without packings. The two types of packing tested (Hiflow and RMSR) yield a similar improvement of the mass transfer.

Nomenclature

A_p (m^2) surface area of silica gel particles
B_{ads} (–) adsorption capacity of silica gel particles
$C^{in}_{H2O,b}$ ($kg.m^{-3}$) concentration of H_2O in the bubble phase entering the FB
$C^{out}_{H2O,b}$ ($kg.m^{-3}$) outlet concentration of H_2O in the bubble phase exiting the FB
$C^{in}_{H2O,e}$ ($kg.m^{-3}$) concentration of H_2O in the emulsion phase entering the FB
$C^{out}_{H2O,e}$ ($kg.m^{-3}$) outlet concentration of H_2O in the emulsion phase exiting the FB
C^{in}_{H2O} ($kg.m^{-3}$) inlet concentration of H_2O to the FB reactor
C^{out}_{H2O} ($kg.m^{-3}$) outlet concentration of H_2O from the FB reactor
$C^{ave}_{H2O,b}$ ($kg.m^{-3}$) average concentration of H_2O in the bubble phase
$C^{ave}_{H2O,e}$ ($kg.m^{-3}$) average concentration of H_2O in the emulsion phase
$C_{H2O,p}$ ($kg.m^{-3}$) concentration of H_2O in the particles
$C_{H2O,s}$ ($kg.m^{-3}$) concentration of H_2O on the surface of particles
D ($m^2.s^{-1}$) molecular gas diffusion coefficient
d_p (m) average particle diameter
F (–) fluidization number
$F(X)$ (–) integral form of $g(X)$
G_{air} ($m^3.s^{-1}$) airflow to the fluidized bed
$g(X)$ (–) extent of conversion
H^{in}_{abs} (t) ($kg.m^{-3}$) inlet absolute humidity value at time t
H^{out}_{abs} ($kg.m^{-3}$) outlet absolute humidity value at time t

Table 6
The average value of different mass-transfer coefficients studied in this work.

No.	packing	Fluidization number (F) (–)	Silica gel (kg)	K_b (s^{-1}) value and increase from unpacked case	K_{tot} (s^{-1})	K_p (s^{-1})	K_e (s^{-1})
1			4	9.04e-5	8.84e-5		
2		1.7	6	6.25e-5	6.15e-5		
3	No packing		8	5.40e-5	5.32e-5		
4		2.3	4	8.30e-5	8.13e-5		
5			6	6.21e-5	6.11e-5		
6			4	10.04e-5 (+15%)	10.14e-5	*0.004*	*803.8*
7		1.7	6	7.32e-5 (+17%)	7.19e-5		
8	RMSR		8	5.60e-5 (+4%)	5.52e-5		
9		2.3	4	9.62e-5 (+16%)	9.39e-5		
10			6	7.66e-5 (+23%)	7.52e-5		
11	Hiflow	2.3	6	7.64e-5 (+23%)	7.50e-5		

K_b (s^{-1}) transfer of H_2O from the emulsion to the bubble phase
k_e $(m.s^{-1})$ transfer of H_2O across the particles' surface and the emulsion gas
K_e (s^{-1}) transfer of H_2O across the particles' surface and the emulsion gas
K_p (s^{-1}) transfer of H_2O from internal particle sites to the particle surface
K_{tot} (s^{-1}) overall transfer of H_2O from the particle to the gas bubbles
$m_{p,dry}$ (kg) weight of dry silica gel particles
$m_{p,sat}$ (kg) weight of saturated silica gel particles
$m_p(t)$ (kg) weight of silica gel particles at each time during the desorption
p_{H2O} (Pa) partial pressure of H_2O
Re (–) Reynolds number
Sc (–) Schmidt number
Sh (–) Sherwood number
t (s) Time
$t_{0.5}$ (s) reaction's half-life
u $(m.s^{-1})$ superficial gas velocity
u_{mb} $(m.s^{-1})$ minimum bubbling velocity
u_{mf} $(m.s^{-1})$ minimum fluidization velocity
V_p (m^3) volume of silica gel particles
V_R (m^3) volume of reactor
X (–) degree of water desorption from silica gel particles at each time

Greek letters

α (–) constant in Eq. (13)
$\dot{m}$ $(kg.s^{-1})$ rate of desorbed water
Δm_{des} (kg) total quantity of desorbed water
ε (–) void fraction in the bed
ε_{mf} (–) void fraction in the bed at minimum fluidizing conditions

CRediT authorship contribution statement

Nasrin Nemati: Writing – review & editing, Writing – original draft, Visualization, Validation, Methodology, Investigation, Formal analysis, Data curation, Conceptualization. **David Pallarès:** Writing – review & editing, Visualization, Validation, Methodology, Conceptualization. **Tobias Mattisson:** Writing – review & editing, Visualization, Validation, Methodology, Conceptualization. **Diana Carolina Guío-Pérez:** Writing – review & editing, Conceptualization. **Magnus Rydén:** Writing – review & editing, Visualization, Validation, Supervision, Resources, Project administration, Methodology, Funding acquisition, Conceptualization.

Declaration of competing interest

The authors declare that they have no known competing financial interests or personal relationships that could have appeared to influence the work reported in this paper.

Data availability

Data will be made available on request.

Acknowledgements

This work has been supported by the Swedish Energy Agency (projects 46525-1 - The application of confined fluidization in energy conversion and P2022-00544 – production of hydrogen and biochar from wood fuels with a new process that utilizes the steam-iron reaction and iron ore concentrate). Fredrik Hildor is acknowledged for valuable discussion and technical help with the TGA experimental setup.

Appendix A. Supplementary data

Supplementary data to this article can be found online at https://doi.org/10.1016/j.powtec.2024.119781.

References

[1] J. Aronsson, E. Krymarys, V. Stenberg, T. Mattisson, A. Lyngfelt, M. Rydén, Improved gas–solids mass transfer in fluidized beds: confined fluidization in chemical-looping combustion, Energy Fuel 33 (5) (2019) 4442–4453, https://doi.org/10.1021/acs.energyfuels.9b00508.
[2] N. Nemati, M. Rydén, Chemical-looping combustion in packed-fluidized beds: experiments with random packings in bubbling bed, Fuel Process. Technol. 222 (2021) 106978, https://doi.org/10.1016/j.fuproc.2021.106978.
[3] N. Nemati, Y. Tsuji, T. Mattisson, M. Rydén, Chemical looping combustion in a packed fluidized bed reactor—fundamental modeling and batch experiments with random metal packings, Energy Fuel (2022), https://doi.org/10.1021/acs.energyfuels.2c00527.
[4] D. Geldart, Types of gas fluidization, Powder Technol. 7 (5) (1973) 285–292, https://doi.org/10.1016/0032-5910(73)80037-3.
[5] S.N. Oka, Fluidized bed combustion, Anthony, E. J., Ed.; CRC Press: Boca Raton, FL, USA, Ottawa, Ontario, Canada, 2003.
[6] D.O. Kunii, Levenspiel, in: H. Brenner (Ed.), Fluidization Engineering, 2nd ed., Butterworth-Heinemann, Newton, MA, USA, 1991.
[7] T. Mattisson, E. Jerndal, C. Linderholm, A. Lyngfelt, Reactivity of a spray-dried NiO/NiAl2O4 oxygen carrier for chemical-looping combustion, Chem. Eng. Sci. 66 (20) (2011) 4636–4644, https://doi.org/10.1016/j.ces.2011.06.025.
[8] T. Chiba, H. Kobayashi, Gas exchange between the bubble and emulsion phases in gas-solid fluidized beds, Chem. Eng. Sci. 25 (9) (1970) 1375–1385, https://doi.org/10.1016/0009-2509(70)85060-6.
[9] J. Aronsson, D. Pallarès, A. Lyngfelt, Modeling and scale analysis of gaseous fuel reactors in chemical looping combustion systems, Particuology 35 (2017) 31–41, https://doi.org/10.1016/j.partic.2017.02.007.
[10] A. Lyngfelt, B. Leckner, A 1000 MWth boiler for chemical-looping combustion of solid fuels – discussion of design and costs, Appl. Energy 157 (2015) 475–487, https://doi.org/10.1016/j.apenergy.2015.04.057.
[11] A. Lyngfelt, A. Brink, Ø. Langørgen, T. Mattisson, M. Rydén, C. Linderholm, 11,000 h of chemical-looping combustion operation—where are we and where do we want to go? Int. J. Greenhouse Gas Control 88 (2019) 38–56, https://doi.org/10.1016/j.ijggc.2019.05.023.
[12] D. Mei, C. Linderholm, A. Lyngfelt, Performance of an oxy-polishing step in the 100 kWth chemical looping combustion prototype, Chem. Eng. J. 409 (2021) 128202, https://doi.org/10.1016/j.cej.2020.128202.
[13] J. Adánez, A. Abad, T. Mendiara, P. Gayán, L.F. de Diego, F. García-Labiano, Chemical looping combustion of solid fuels, Prog. Energy Combust. Sci. 65 (2018) 6–66, https://doi.org/10.1016/j.pecs.2017.07.005.
[14] T.W. Asegehegn, M. Schreiber, H.J. Krautz, Investigation of bubble behavior in fluidized beds with and without immersed horizontal tubes using a digital image analysis technique, Powder Technol. 210 (3) (2011) 248–260, https://doi.org/10.1016/j.powtec.2011.03.025.
[15] H.V. Nguyen, O.E. Potter, A.B. Whitehead, Bubble distribution and eruption diameter in a fluidized bed with a horizontal tube bundle, Chem. Eng. Sci. 34 (9) (1979) 1163–1164, https://doi.org/10.1016/0009-2509(79)85024-1.
[16] W. Mojtahedi, Effect of an immersed tube-Bank in a gas Fluidized bed, Int. J. Heat Mass Transf. 30 (6) (1987) 1095–1101, https://doi.org/10.1016/0017-9310(87)90039-1.
[17] S. Andersson, F. Johnsson, B. Leckner, Fluidization regimes in non-slugging fluidized beds, in: Proceedings, 1989, pp. 239–242.
[18] G.L. Matheson, Process for Contacting Solids and Gases 2533026, 1950.
[19] K.D. Williamson, Design and Mass Transfer Study for New Multistage Fluidization Reactor, Chemical Engineering, The Pennsylvania State University, Pennsylvania, 1961.
[20] J.P. Sutherland, G. Vassilatos, H. Kubota, G.L. Osberg, The effect of packing on a fluidized bed, AICHE J. 9 (4) (1963) 437–441, https://doi.org/10.1002/aic.690090406.
[21] W.K. Kang, J.P. Sutherland, G.L. Osberg, Pressure fluctuations in a fluidized bed with and without screen cylindrical packings, Ind. Eng. Chem. Fundam. 6 (4) (1967) 499–504.
[22] E.N. Ziegler, W.T. Brazelton, Radial heat transfer in a packed-fluidized bed, Ind. Eng. Chem. Process Design Developm. 2 (4) (1963) 276–281.
[23] J.D. Gabor, Lateral solids mixing in Fludized-packed beds, AICHE J. 10 (3) (1964) 345–350, https://doi.org/10.1002/aic.690100313.
[24] J.D. Gabor, W.J. Mecham, Radial gas mixing in fluidized-packed beds, Ind. Eng. Chem. Fundam. 3 (1) (1964) 60–65.
[25] J.D. Gabor, W.J. Mecham, Engineering development of fluid-bed fluoride volatility processes, Part 4. Fluidized-packed beds: studies of heat transfer, solid gas mixing, and elutriation, in: AEC Research and Development Report; Chemical Separation Processes for Plutonium and Uranium, 1965, pp. 1–127.
[26] L.J. Anastasia, J.D. Gabor, W.J. Mecham, Engineering Development of Fluid-Bed Fluoride Volatility Processes Part 3, Fluid-Bed Fluorination of Uranium Dioxide Fuel Pellets, 1965.
[27] J.D. Gabor, Lateral transport in a fluidized-packed bed: Part I. Solids mixing, AICHE J. 11 (1) (1965) 127–129, https://doi.org/10.1002/aic.690110126.

[28] J.D. Gabor, B.E. Stangeland, W.J. Mecham, Lateral transport in a fluidized-packed bed: Part II. Heat transfer, AICHE J. 11 (1) (1965) 130–132, https://doi.org/10.1002/aic.690110127.
[29] G. Donsì, G. Ferrari, B. Formisani, Expansion behaviour of confined fluidized beds of fine particles, Can. J. Chem. Eng. 67 (2) (1989) 185–190, https://doi.org/10.1002/cjce.5450670204.
[30] G. Donsì, G. Ferrari, B. Formisani, G. Longo, Confined fluidization of fine particles in a packed bed of coarse particles: model and experimental description, Powder Technol. 61 (1) (1990) 75–85, https://doi.org/10.1016/0032-5910(90)80068-A.
[31] D. Ziółkowski, J. Michalski, Onset of fluidization of fines in an organized system within voids of packings formed of spherical elements, Chem. Eng. Sci. 47 (15–16) (1992) 4007–4016, https://doi.org/10.1016/0009-2509(92)85150-A.
[32] B. Buczek, P. Zabierowski, Confined fluidization of fines in fixed bed of coarse particles, Chem. Process. Eng. 37 (4) (2016) 545–557, https://doi.org/10.1515/cpe-2016-0044.
[33] R.J. Farrell, E.N. Ziegler, Kinetics and mass transfer in a fluidized packed-bed: catalytic hydrogenation of ethylene, AICHE J. 25 (3) (1979) 447–455, https://doi.org/10.1002/aic.690250309.
[34] N. Nemati, P. Andersson, V. Stenberg, M. Rydén, Experimental investigation of the effect of random packings on heat transfer and particle segregation in packed-fluidized bed, Ind. Eng. Chem. Res. 60 (28) (2021) 10365–10375, https://doi.org/10.1021/acs.iecr.1c01221.
[35] K. Qin, H. Thunman, B. Leckner, Mass transfer under segregation conditions in fluidized beds, Fuel 195 (2017) 105–112, https://doi.org/10.1016/j.fuel.2017.01.021.
[36] J. Aronsson, D. Pallarès, M. Rydén, A. Lyngfelt, Increasing gas–solids mass transfer in fluidized beds by application of confined fluidization—a feasibility study, Appl. Sci. 9 (4) (2019) 634, https://doi.org/10.3390/app9040634.
[37] Q. Zafar, A. Abad, T. Mattisson, B. Gevert, M. Strand, Reduction and oxidation kinetics of Mn3O4/mg–ZrO2 oxygen carrier particles for chemical-looping combustion, Chem. Eng. Sci. 62 (23) (2007) 6556–6567, https://doi.org/10.1016/j.ces.2007.07.011.
[38] F. Scala, Mass transfer around freely moving active particles in the dense phase of a gas fluidized bed of inert particles, Chem. Eng. Sci. 62 (16) (2007) 4159–4176, https://doi.org/10.1016/j.ces.2007.04.040.
[39] D. Mei, H. Zhao, S. Yan, Kinetics model for the reduction of Fe 2 O 3 /Al 2 O 3 by CO in chemical looping combustion, Chem. Eng. Process. Process Intensif. 124 (2018) 137–146, https://doi.org/10.1016/j.cep.2017.12.013.
[40] S. Vyazovkin, A.K. Burnham, J.M. Criado, L.A. Pérez-Maqueda, C. Popescu, N. Sbirrazzuoli, ICTAC kinetics committee recommendations for performing kinetic computations on thermal analysis data, Thermochim. Acta 520 (1–2) (2011) 1–19, https://doi.org/10.1016/j.tca.2011.03.034.
[41] J.H. Sharp, G.W. Brindley, B.N.N. Achar, Numerical data for some commonly used solid state reaction equations, J. Am. Ceram. Soc. 49 (7) (1966) 379–382, https://doi.org/10.1111/j.1151-2916.1966.tb13289.x.
[42] A. Hayhurst, M. Parmar, Measurement of the mass transfer coefficient and Sherwood number for carbon spheres burning in a bubbling fluidized bed, Combust. Flame 130 (4) (2002) 361–375, https://doi.org/10.1016/S0010-2180(02)00387-5.
[43] L. Guo, H. Zhao, K. Wang, D. Mei, Z. Ma, C. Zheng, Reduction kinetics analysis of sol–gel-derived CuO/CuAl2O4 oxygen carrier for chemical looping with oxygen uncoupling, J. Therm. Anal. Calorim. 123 (1) (2016) 745–756, https://doi.org/10.1007/s10973-015-4904-6.